10 Nov 2023

Modeling Hydration Kinetics Of Sustainable Cementitious Binders Using An Advanced Nucleation And Growth Approach

Taihao Han

Jie Huang
Missouri University of Science and Technology, jieh@mst.edu

Gaurav Sant

Narayanan Neithalath

et. al. For a complete list of authors, see https://scholarsmine.mst.edu/ele_comeng_facwork/5124

Recommended Citation

Modeling hydration kinetics of sustainable cementitious binders using an advanced nucleation and growth approach

Taihao Han [a,*], Jie Huang [b], Gaurav Sant [c], Narayanan Neithalath [d], Ashutosh Goel [e], Aditya Kumar [a]

[a] Department of Materials Science and Engineering, Missouri University of Science and Technology, 140 McNutt Hall, 1400 N Bishop, Rolla, MO 65409, USA
[b] Department of Electrical and Computer Engineering, Missouri University of Science and Technology, Rolla, MO 65409, USA
[c] Department of Civil and Environmental Engineering, University of California, Los Angeles, Los Angeles, CA 90095, USA
[d] School of Sustainable Engineering and the Built Environment, Arizona State University, Tempe, AZ 85287, USA
[e] Department of Materials Science and Engineering, Rutgers, The State University of New Jersey, NJ 08854, USA

A B S T R A C T

Supplementary cementitious materials (SCMs) are utilized to partially substitute Portland cement (PC) in binders, reducing carbon-footprint and maintaining excellent performance. Nonetheless, predicting the hydration kinetics of [PC + SCM] binders is challenging for current analytical models due to the extensive diversity of chemical compositions and molecular structures present in both SCMs and PC. This study develops an advanced phase boundary nucleation and growth (pBNG) model to yield *a priori* predictions of hydration kinetics—i.e., time-resolved exothermic heat release profiles—of [PC + SCM] binders. The advanced pBNG model integrates artificial intelligence as an add-on, enabling it to accurately simulate hydration kinetics for [PC + SCM] binders. This study utilizes a database that includes calorimetry profiles of 710 [PC + SCM] binders, encompassing a diverse range of commonly-used SCMs as well as both commercial and synthetic PCs. The results show that the advanced pBNG model predicts the heat evolution profiles of [PC + SCM] in a high-fidelity manner.

1. Introduction

With the steady growth of the global population and rural-to-urban migration, there is an ever-increasing demand for Portland cement (PC) for use in infrastructure construction, repair, and rehabilitation. Every year, the PC manufacture contributes to 9% of anthropogenic CO_2 emissions [1–3], which accelerates global warming as well as its associated manifestations (e.g., rising sea levels; increase in frequency and severity of natural disasters; etc.). CO_2 emissions from the cement industry are attributed to two reasons: decomposition of $CaCO_3$ (a cement precursor); and combustion of fossil fuels (e.g., coal, oil, etc.). To produce PC clinker, the raw materials must be heated to ∼ 1500 °C. This high temperature is necessary to form the main constituent of cement clinker, known as alite (C_3S; where: C = CaO; S = SiO_2; A = Al_2O_3; $ = SO_3; and H = H_2O). Some cement manufacturers [4,5] have developed and employed manufacturing technologies that utilize renewable energy—instead of CO_2-intensive fossil fuels—for the production of PC clinker. However, these innovative technologies are not yet widely adopted by production plants, primarily due to high capital and

operational costs. Governments have encouraged manufacturers to install CO_2 capture-and-storage technologies to reduce emissions, but only a few manufacturers have done so due to the high costs involved [6]. As an alternative, reducing the use of PC in cementitious binders (e.g., mortars and concrete) is a more plausible solution—at least in the short term—to reducing its carbon-footprint. There are two potential methods to reduce the use of PC in infrastructure without sacrificing performance: use of alternative cements (instead of PC); and replacement of PC with supplementary cementitious materials (SCMs). Use of alternative cements is appealing, as it fully replaces PC with a more sustainable counterpart (e.g., geopolymer [7]; calcium sulfoaluminate cement [8]; magnesium oxychloride cement [9]). However, due to our incomplete understanding of hydration kinetics, microstructural evolution, and property evolution in alternative cementitious binders, it is a challenge for manufacturers to produce alternative cements that would satisfy rather strict construction and compliance criteria. Based on state-of-art of research and practice in the field, the use of SCMs as partial replacement of PC is more prevalent. In cementitious binders, SCMs can potentially substitute up to 60% of PC. The common SCMs are: fly ash

(FA); limestone (LS); slag; metakaolin (MK); silica fume (SF); and quartz (QZ) [10–14]. Chemistry and content of SCMs can substantially alter mechanical properties [14,15], hydration kinetics [16,17], and rheology [14,18] of PC-based systems. Comprehensive research on evaluating, cataloging, and elucidating the influences of SCMs on properties of PC binders is important for developing sustainable cementitious binders.

Hydration kinetics is the most vital property of PC because it can be used to estimate—if not accurately, at least crudely—other properties (e. g., degree of hydration; compressive strength; set time; rheology; and durability). SCMs affect PC hydration through several mechanisms, the origins of which can be traced back to the SCM's physical and chemical characteristics. SCMs can act as fillers, providing additional surfaces for heterogeneous nucleation and the ensuing growth of the main hydration product (or hydrate), calcium silicate hydrate (C-S-H) [19,20]. However, if the SCM particulates are small (median particle size $\lesssim 1$ μm), the filler effect may be diminished due to coagulation and agglomeration of the particulates [17,21]. SCMs with high aluminate content may suppress PC hydration by releasing $Al(OH)_4^-$ [16,17,22]. The $Al(OH)_4^-$ species can absorb onto surfaces of PC and SCM particles, thereby preventing them from coming into contact with water, and suppressing their ability to dissolve or participate in nucleation and growth of C-S-H and other hydrates. Furthermore, aluminosilicate SCMs—upon dissolution—can release silicate ions (e.g., $H_3SiO_4^-$; $H_2SiO_4^{2-}$), which can react with portlandite (CH) to form additional C-S-H via a process known as the pozzolanic reaction [16,17,22]. Sulfate dissolved from SCMs (e.g., fly ash) also can absorb onto PC particles and inhibit the hydration of PC's major phase, alite. Furthermore, sulfur reacts with C_3A to form additional ettringite and monosulfoaluminate, which consume calcium ions, thereby decelerating the hydration of alite and precipitation of C-S-H [23,24]. Moreover, the aqueous reactivity of SCMs varies over a wide range owing to their diverse chemical compositions and molecular structures. Due to such intricate influences of SCMs, the pathway of developing theory-based models that produce high-fidelity predictions of hydration kinetics—i.e., time-resolved exothermic heat release profiles—of [PC + SCM] remains unclear. Many studies [25–31] have attempted to investigate simple PC binders (e.g., C_3S and C_3S-C_3A-gypsum binders) and develop theory-based models to predict their hydration kinetics. Although these studies have demonstrated a comprehensive understanding of correlations between mixture design and hydration kinetics of simple binders, such knowledge fails to interpret highly nonlinear and mutually-interacting processes in the more complex [PC + SCM] systems that have substantially greater degrees of freedom and larger number of parameters that can influence the hydration behavior. Simply put, the models developed for simple binders cannot produce reliable predictions of hydration kinetics for complex [PC + SCM] [32–35].

The dominant mechanism of the hydration of PC is phase boundary nucleation and growth (pBNG) [30,36–38]. Several studies [19,30,39–41] have developed numerical models to reproduce hydration kinetics of cementitious materials based on the pBNG mechanism, which assumes C-S-H is the sole hydrate with a constant density. The first pBNG model, developed by Thomas [41], was premised on the hypothesis that the driving mechanism for PC hydration is the time-dependent nucleation of C-S-H on and around PC particles, followed by its isotropic growth at a constant rate. However, further studies and experiments indicated that the formation of C-S-H was more complex than initially thought, and that it involved a short burst of heterogenous nucleation—akin to a singular *site-saturation* nucleation event—on surfaces of PC particles. Scherer et al. [39,42] modified the pBNG model by incorporating heterogeneous, *site-saturation* nucleation and anisotropic growth of C-S-H along with other mechanisms (e.g., chemical shrinkage) that affect PC hydration kinetics. However, this model had some drawbacks, including the assumption of a constant growth rate of C-S-H which did not agree with experiments, and the inability to simulate hydration kinetics of [PC + SCM] binders. These—and other—limitations were addressed in recent modifications of the pBNG

model [16,22,38,43–45]. The modified pBNG model incorporates several features to accurately reproduce heat evolution profiles of [PC + SCM], including a growth rate that changes with time to mimic the experimentally-observed temporal variations in supersaturation of C-S-H. This process begins with heterogeneous nucleation of C-S-H on the surfaces of PC and SCM particles, followed by outward, anisotropic growth of the nuclei into the contiguous capillary pore space with a time-varying rate. As the hydrates impinge onto other hydrates and anhydrous (unreacted) PC and SCM particles, and the abundance of ionic species in the solution declines, the hydration rate slows down. However, the time-varying growth rate of C-S-H is one of the free parameters of the pBNG model; and, to obtain these free parameters, either complex and cumbersome experiments (e.g., scanning transmission electron microscope [46]) need to be conducted, or the values simply need to be estimated (e.g., best guess) and refined through trial-and-error based optimizations. Because of this, the modified pBNG model—while good at reproducing hydration kinetics of cementitious binders and extracting the time-dependent growth rate of C-S-H from experimentally-measured calorimetry profiles—is unable to produce *a priori* predictions of new PC binders.

In past decades, artificial intelligence has proven to be a highly effective tool for predicting properties of cementitious materials. Numerous studies have utilized machine learning (ML) models to predict mechanical properties [47–52], rheological properties [53,54], and hydration kinetics [32–35] of PC. Therefore, we hypothesize that ML models can be used to guess (predict) the free parameters of the pBNG model, such as the time-dependent C-S-H growth rate. Furthermore, we hypothesize that the advanced pBNG model integrating ML as an add-on can compensate for the shortcomings of conventional models and yield reliable, *a priori* predictions of hydration kinetics of [PC + SCM] that ensure compliance with fundamental materials laws (e.g., kinetic mechanisms). Here, the pBNG component distills the calorimetry profiles of hundreds of [PC + SCM] into a database of simple, monotonous time-dependent C-S-H growth rate profiles. This database is used to train the ML component; and subsequently, the ML model predicts C-S-H growth rate profiles for new [PC + SCM]. Finally, by knowing C-S-H growth rate profiles of new [PC + SCM], the pBNG component calculates their heat evolution profiles. Through this merger, *a priori* and *parameter-free* predictions of calorimetry profiles of [PC + SCM] are possible.

In this paper, we develop an advanced pBNG model that integrates a deep forest (DF) model to yield predictions of time-dependent calorimetry profiles of sustainable cementitious binders. Emphasis is given to predict the first 24 h of cement hydration; since, within this early-age period, cement hydration transitions through multiple mechanisms including dissolution, induction period, and nucleation and growth of the hydrates. Furthermore, focus is given to predict the differential heat flow rate profiles—rather than the cumulative heat release profiles—because: the former is more sensitive to changes in the driving mechanism of hydration (e.g., from dissolution to induction period and then to acceleration up to the peak); and can be readily integrated with respect to time to obtain cumulative heat release profiles. The research is conducted based on a database contains 710 [PC + SCM] binders, including a wide range of common SCMs (i.e., QZ, LS, FA, MK, and SF.) and both commercial cement (CC) and synthetic cement (SC). The advanced pBNG model predicts heat flow rate profiles of [PC + SCM] in a high-fidelity manner based on their mixture designs. This study also aims to understand the influence of SCMs on calorimetry profiles and growth rates of C-S-H. Overall, this study develops a novel, theory-guided prediction tool to understand and predict hydration behaviors of complex [PC + SCM] systems, thereby aiding in the design and discovery of sustainable cementitious materials.

2. Modeling method

2.1. Phase boundary nucleation and growth model

The pBNG model is kinetic model to simulate the heat evolution profiles of [PC + SCM] binders. This section presents a brief information about the pBNG model; further details can be found elsewhere [16,38,43]. Among the four anhydrous phases (C_3S; C_3A; C_2S; and C_4AF) present in PC, C_2S and C_4AF exhibit a low intrinsic dissolution rate, and do not contribute significantly to early-age hydration of PC [23,39,55]. In contrast, C_3A and gypsum rapidly react and form ettringite in the first couple minutes after mixing, releasing a substantial amount of heat [27,56,57]. After the initial burst of nucleation and rapid growth, ettringite precipitation slows down dramatically [27,56,57]. In the pBNG model, C_3S reacts with water to form C-S-H, which is the primary hydration product and has a constant density [19,39–41]. C-S-H nucleates and grows on boundaries of solid phases (i.e., PC and SCM surfaces). The rate-controlling mechanism is *site saturation* nucleation and growth of C-S-H; and therefore, the pBNG model assumes that a fixed number of nuclei are formed during the initial nucleation burst, and no further nuclei are allowed to form after this point [58,59]. Based on those assumptions, **Eq. (1)** [16,38,43,44,60] shows the volume fraction [$X(t)$, unitless] of C-S-H at any given time (t, hour).

$$X(t) = 1 - \exp\left(-2r_G \bullet G_{out}(t) \bullet a_{BV} \bullet t \bullet \left(1 - \frac{F_D\left(G_{out}(t) \bullet \sqrt{\pi \bullet g \bullet I_{density}} \bullet t\right)}{G_{out}(t) \bullet \sqrt{\pi \bullet g \bullet I_{density}} \bullet t} \right) \right) \quad (1)$$

Herein, F_D is the f-Dawson function [61]. The growth rate of C-S-H is anisotropic, with a faster rate in the direction perpendicular to solid surfaces than in the lateral direction. The variable G_{out} ($um.h^{-1}$) is the outward (perpendicular direction) growth rate of C-S-H. G_{out} ($um.h^{-1}$) changes with respect to time, which allows the pBNG model to account for the changes in the degree of saturation of C-S-H [16,38,43,44,60].

It should be noted that C-S-H cannot grow and penetrate into solid surfaces at the early age of hydration [39,42]. Consequently, the multiplier r_G (≈ 0.5 [16,38], unitless) is applied to compensate for the growth rate toward the surface. The variable g (≈ 0.25, unitless) is a constant (**Eq. (2)** to reproduce the needle-like geometry of C-S-H observed in experiments. Previous studies [16,42] have shown that the ratio of the growth rate of outward direction (G_{out}) to lateral direction (G_{par}) is a constant ratio (2:1). The variable $I_{density}$ is nucleation density (um^{-2}), the number of C-S-H nuclei per unit surface area of solids. In the pBNG model, the nucleation density is assumed as constant for C-S-H (i. e., 12 [38,60]). The variable a_{BV} (um^{-1}) is the boundary area per unit volume of solids, shown in **Eq. (3)**. **Eq. (3)** contains three sub-equations to calculate a_{BV} in plain, binary, and ternary binders. Therein, w/b (unitless) is the water-to-binder ratio. The binder's volume is equal to the total volume of solid (i.e., PC and SCMs). The binder area (SSA_{binder}, $cm^2.g^{-1}$) is the available solid area for producing nuclei C-S-H, which is calculated in **Eq. (4)**. **Eq. (4)** contains three sub-equations to calculate SSA_{binder} in plain, binary, and ternary binders. The variable ρ ($g.cm^{-1}$) is the density; and SSA_i ($cm^2.g^{-1}$) is the specific surface area of PC and SCM solids. The variable a_{scm} (unitless) is the fraction of effective surface area of the SCM. Here, due to the agglomeration or ion-specific effects (i. e., sulfate and $Al(OH)_4^-$), the acceleration of hydration caused by the filler effect of the SCM could be diminished; and a_{scm} accounts for this effect [16,62,63].

$$g = \left(\frac{G_{par}(t)}{G_{out}(t)} \right)^2 \quad (2)$$

$$\begin{cases} a_{BV} = \left(\dfrac{SSA_{binder}}{\dfrac{w}{b} + \dfrac{1}{\rho_{cement}} + \dfrac{1}{z_{scm1}} \bullet \dfrac{1}{\rho_{scm1}} + \dfrac{1}{z_{scm2}} \bullet \dfrac{1}{\rho_{scm2}}} \right) \\[3em] a_{BV} = \left(\dfrac{SSA_{binder}}{\dfrac{w}{b} + \dfrac{1}{\rho_{cement}} + \dfrac{1}{z_{scm1}} \bullet \dfrac{1}{\rho_{scm1}}} \right) \\[3em] a_{BV} = \left(\dfrac{SSA_{binder}}{\dfrac{w}{b} + \dfrac{1}{\rho_{cement}}} \right) \end{cases} \quad (3)$$

$$\begin{cases} SSA_{binder} = SSA_{cement} + a_{scm1}SSA_{scm1}\dfrac{z_{scm1}}{100 - z_{scm1}} + a_{scm1}SSA_{scm2}\dfrac{z_{scm2}}{100 - z_{scm2}} \\[1.5em] SSA_{binder} = SSA_{cement} + a_{scm1}SSA_{scm1}\dfrac{z_{scm1}}{100 - z_{scm1}} \\[1.5em] SSA_{binder} = SSA_{cement} \end{cases} \quad (4)$$

Previous studies [16,38,60] have shown that the degree of hydration [$\alpha(t)$, unitless] of PC is linearly related to the volume fraction of C-S-H. This correlation is shown in **Eq. (5)**. The variable B (unitless) is a constant described in **Eq. (6)**, where ρ_{CSH} is the density of C-S-H (2.07 g. cm^{-3} [64,65]) and c (=-7.04 × 10^{-2}) is chemical shrinkage over the course of hydration.

$$\alpha(t) = B \bullet X(t) \quad (5)$$

$$B = \left(\frac{\frac{\rho_{cement}}{\rho_{CSH}}}{\frac{w}{b} \bullet \rho_{cement}}{\rho_{water}} + 1} \bullet \frac{c + \frac{1}{\rho_{cement}} - \frac{1}{\rho_{water}}}{\frac{1}{\rho_{CSH}} - \frac{1}{\rho_{water}}} \right)^{-1} \quad (6)$$

With the aforementioned equations and assumptions, the pBNG model requires two variables (i.e., a_{scm} and G_{out}) to be optimized to simulate the hydration kinetics of [PC + SCM]. The variable a_{scm} is determined based on physicochemical properties of SCMs as explained in our prior studies [16,22,38,43]. G_{out} is a time-dependent variable, which can be obtained from calorimetry profiles by using pBNG model with the Nelder-Mead-based simplex algorithm [66,67]. Fig. 1 shows that the pBNG model can accurately reproduce heat evolution profiles of [PC + SCM] when given the values of a_{scm}, G_{out} and other experimentally-measured parameters pertaining to the mixture design and physicochemical properties of precursors. In this study, we used a DF model to predict G_{out} for new [PC + SCM] systems; and then used G_{out} as an input in the pBNG model to predict the systems' heat evolution profiles.

2.2. Advanced pBNG model

In this study, an advanced pBNG model is developed to accurately predict heat evaluation profiles of [PC + SCM]. The model incorporates DF component (description can be found in **Section S1.2**) to guess the C-S-H grow rate and then simulates heat evaluation profiles. Fig. 2 shows the architecture of the advanced pBNG model. After the database is collected from experiment, the database is split into training and testing datasets. Then, based on the physicochemical properties of precursors, pBNG model calculates C-S-H growth rate profiles for [PC + SCM] in the training dataset. Subsequently, the DF component of the advanced pBNG model learns input–output correlations from the C-S-H growth rate profiles and leverages such knowledge to predict the C-S-H growth
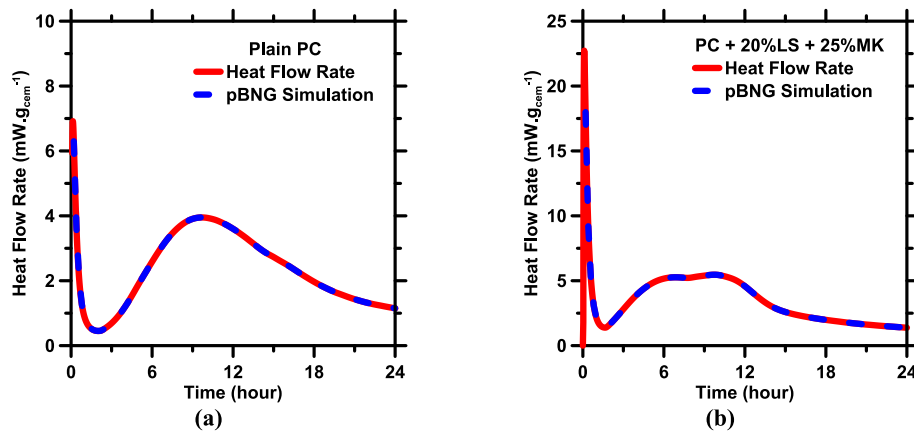
Fig. 1. Representative simulated and measured heat flow rate profiles of (a) plain PC and (b) [PC + LS + MK] binders. The simulated profiles are obtained from the pBNG model.
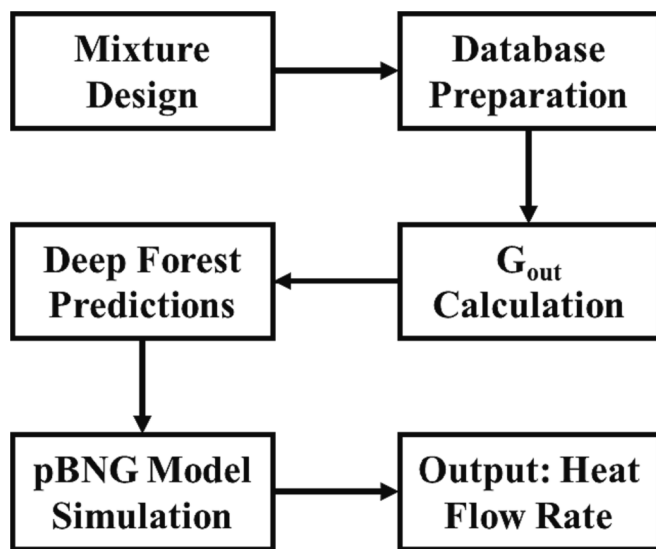

Fig. 2. Schematic of the advanced pBNG model that is used to predict heat evolution profiles of [PC + SCM].

rate profiles for the testing dataset. The predicted C-S-H growth rate profiles are implemented in the pBNG component to reproduce heat flow rate profiles. It is worth noting that the fraction of effective surface area for each SCM is a critical parameter that must be manually determined, with the fraction of effective surface area of each SCM listed in Table S1. All surfaces of QZ and LS can nucleate C-S-H. Due to the agglomeration, the effective surface area of SF substantially decreases. Additionally, the filler effect from MK and FA is compensated by Al(OH)$_4^-$ suppressing the hydration. The reactivity and SO$_3$ content of each FA also play a role in determining the specific fraction of effective surface area assigned to them.

3. Database collection

Heat evolution profile database of [PC + SCM] is collected from our previous studies [32–35]. The database consists of heat flow rate profiles of 710 [PC + SCM] binders (i.e., plain; binary; and ternary binders). The SCMs include QZ, LS, MK, SF, and FA. The binary binders (PC + 1 SCM) contain all SCMs, and the ternary binders (PC + 2 SCMs) include the combination of all SCMs except for FA. The database consists of 10 types of PCs [3 commercial cements (CCs); and 7 synthetic cements (SCs)] and 10 types of FAs. The chemical compositions and physical properties of

SCMs and PCs are shown in Tables S1 and S2, respectively.

The parent database is separated into two distinct datasets: the training dataset, which comprises 79,200 data-records from 660 [PC + SCM] binders, and the testing dataset, which contains 6,000 data-records from 50 [PC + SCM] binders. The training dataset is utilized to train the DF model, allowing it to learn input–output correlations and optimize hyperparameters. Subsequently, the performance of the ML model is evaluated using the testing dataset to assess its accuracy in predicting heat flow rate profiles. To evaluate the ML models, five statistical parameters, including the coefficient of determination (R^2), Pearson correlation coefficient (R), mean absolute error (MAE), root mean squared error ($RMSE$), and mean absolute percentage error ($MAPE$), are employed. Both datasets include physicochemical attributes of binders as inputs: C$_3$S content (%$_{mass}$); C$_2$S content (%$_{mass}$); C$_3$A content (%$_{mass}$); C$_4$AF content (%$_{mass}$); C$\$$H$_2$ content (%$_{mass}$); water-to-solid ratio (unitless); content of each SCM (%$_{mass}$); specific surface area (SSA) of PC and SCMs (cm^2. g^{-1}); *number of constraints* of FA (unitless); SO$_3$ content of FA (%$_{mass\ of\ ASM}$); and time (hour). The hydration time is 0-to-24 h, and the interval step is 0.2-hour. The *number of constraints* is a parameter to evaluate the aqueous reactivity of FA. The reactivity of FAs in PC depends on their chemical compositions and molecular structures, which can vary in a wide range. Generally, FAs with high values of *number of constraints* exhibit low aqueous reactivity due to containing a large volume of crystalline structure and vice versa. The detail and equations for *number of constraints* can be founded in our previous studies [68,69]. Furthermore, Weerdt et al. [70] and Han et al. [35] have found that SO$_3$ from FA can significantly alter the hydration kinetics of PC. Therefore, it is important to use the SO$_3$ content of FA as an input variable to improve the prediction accuracy. The output of model is the time-dependent heat flow rate (mW. g$^{-1}_{Cem}$) of [PC + SCM]. Statistical parameters pertaining to input and output variables are shown in Tables S3 and S4.

4. Results and discussion

For a 24-hour hydration period with a 0.2-hour step size, the DF model was utilized to yield predictions of heat flow rate profiles for [PC + SCM] in the testing dataset for a 24-hour hydration period with a 0.2-hour step size. The prediction performance from the DF model is employed as a benchmark for evaluating and compare the performance of the advanced pBNG model. Fig. 3 demonstrates a comparison between predicted heat evaluation profiles of representative binders and the experimental measurements. The model's accuracy and reliability are evaluated using statistical parameters, which are provided in Table 1 and offer a quantitative measure of how well the model's predictions match the experimental measurements. Based on the results shown in
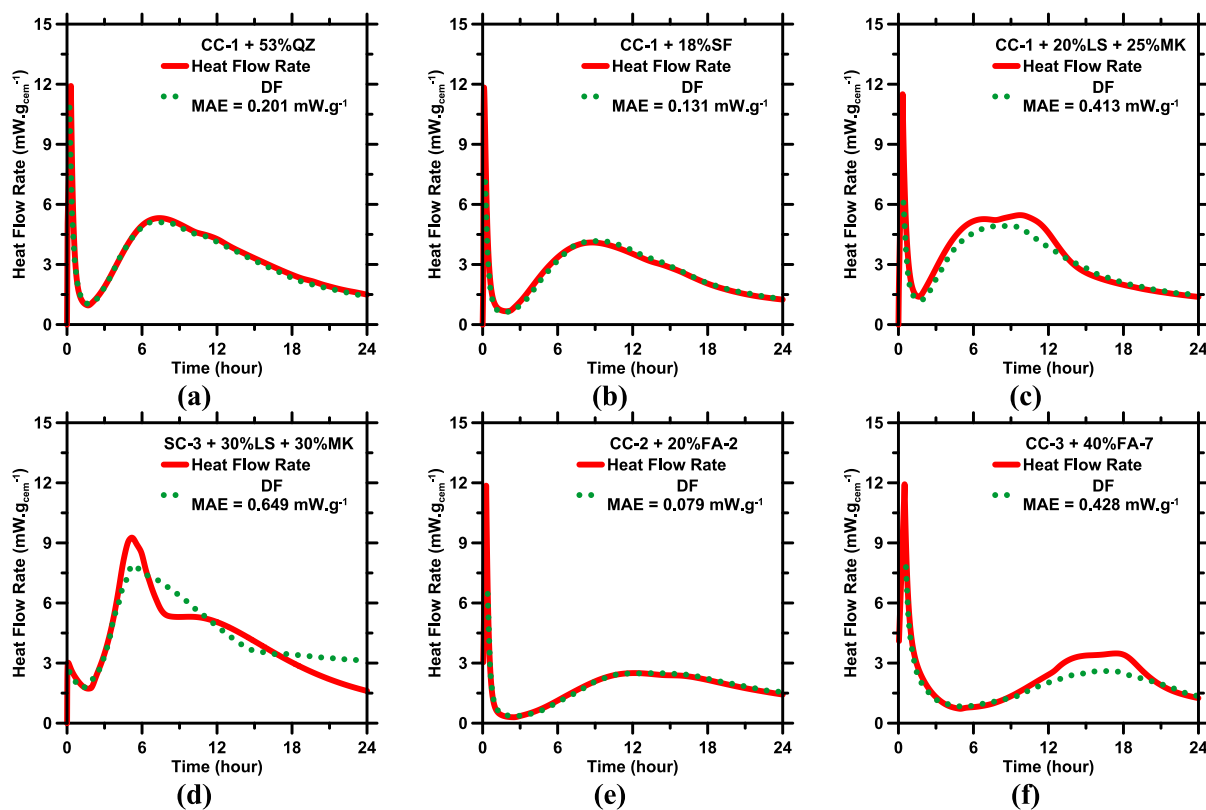
Fig. 3. The standalone DF's predictions of heat flow rate profiles for representative binders: **(a)** [CC-1 + QZ]; **(b)** [CC-1 + SF]; **(c)** [CC-1 + LS + MK]; **(d)** [SC-3 + LS + MK]; **(e)** [CC-2 + FA-2]; and **(f)** [CC-3 + FA-7] compared against experimental measurements. Mean absolute error (*MAE*) of each prediction is shown in legends.

Table 1

An analysis of the prediction accuracy of the standalone DF and DF-pBNG models on heat flow rate profiles of [PC + SCM] over 24 h hydration, utilizing five statistical parameters as a measure of performance.

ML Model	R	R^2	MAE	MAPE	RMSE
	Unitless	*Unitless*	mW. g_{cem}^{-1}	%	mW. g_{cem}^{-1}
DF	0.8247	0.8552	0.3701	17.45	0.7514
DF-pBNG	0.9999	0.9999	0.0106	0.38	0.0161

Table 1 and Fig. 3, the standalone DF model can produce predictions of heat flow rate profiles with reasonable accuracy, as evidenced by $R^2 \approx 0.86$ and $RMSE \approx 0.75$ mW.g_{cem}^{-1}. However, it can be observed in Fig. 2 that the DF does not perform well in predicting heat flow rate at hydration peaks and during the early hours (<12 h) of hydration. This can be attributed to three reasons. Firstly, the hydration transitions through three stages (i.e., initial period; induction period; and acceleration period) in the first 12 h, each with unique hydration behaviors and distinct mechanisms. This results in two inflection points in the heat evolution profiles, where the concavity of the profiles changes rapidly, leading to sudden changes in hydration kinetics. The complexity of those structures makes it challenging for the DF model to accurately capture the overall trend in the first 12 h of hydration. The second reason is that SCMs cast unique influences on the hydration of PC, depending on their chemical compositions, fineness, and molecular structures. The influences of each SCM on hydration kinetics are demonstrated in the later sections. Due to the effects of SCMs, it is a challenge for the DF model to capture the global trend in the heat evaluation profiles. Third, the DF model operates solely on mathematical approaches without taking into account any material laws, where outputs may violate fundamental material laws and, as a results, decrease prediction accuracy.

The performance of the advanced pBNG model in predicting heat flow rate profiles of representative [PC + SCM] is demonstrated in

Fig. 4. The performance of the model is further evaluated using statistical parameters listed in Table 1. To facilitate a straightforward comparison, Fig. 4 also includes the predictions made by the DF model as the benchmark. The predictions for the remaining binders can be found in Fig. S1.

The predictions produced from the advanced pBNG model, as seen in Table 1 and Fig. 4, demonstrate exceptional accuracy in predicting heat flow rate profiles, with $R^2 \approx 0.99$ and $RMSE \approx 0.02$ mW.g_{cem}^{-1}. The errors made by the model are minimal. The advanced pBNG model also successfully captures the hydration peak, which is the most critical juncture for understanding the hydration behavior of [PC + SCM]. At the hydration peak, cement binders begin to set and gain strength in a short time due to the formation of large amounts of hydrates [23,71–73]. As such, the ability to accurately capture the hydration peak is often considered the primary (or even sole) parameter for evaluating the performance of kinetic models [19,30,38,39,74]. The accurate predictions produced by the advanced pBNG model can be credited to two reasons. Firstly, in contrast to the DF model, the pBNG component produce the final outputs through kinetic theories, preventing any violations of fundamental material laws. This, in turn, bolsters the reliability of predicted heat flow profiles. Secondly, the DF component estimates the C-S-H growth rate profiles in a high-fidelity manner. It is crucial to recognize that the pBNG component exhibits a strong sensitivity to C-S-H growth rate, wherein even minor variations can substantially influence hydration kinetics. Given the straightforward structure of C-S-H growth rate profiles, the DF component is easy to capture input–output correlations, effectively reducing the demand for computational resources (i.e., memory and learning time). Fig. 5 directly compares the structures of heat flow rate and C-S-H growth profiles. As seen in the figure, these growth rate profiles are far simpler than heat flow rate profiles, with a monotonic decrease over time and no sharp inflection points. Despite the simple (i.e., monotonous) nature of growth rate profiles, they retain all crucial information about hydration
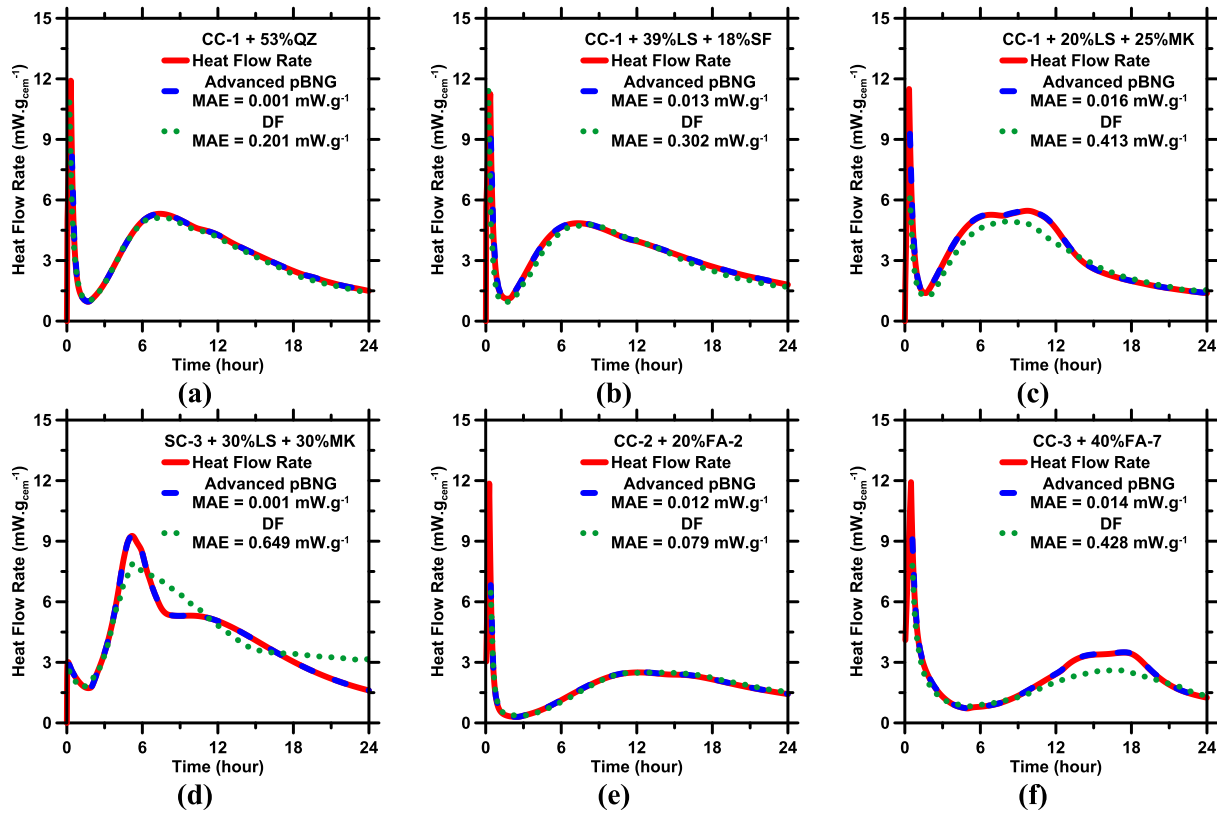
Fig. 4. The predictions of heat flow rate profiles as produced by advanced pBNG and DF models for representative binders: **(a)** [CC-1 + QZ]; **(b)** [CC-1 + SF]; **(c)** [CC-1 + LS + MK]; **(d)** [SC-3 + LS + MK]; **(e)** [CC-2 + FA-2]; and **(f)** [CC-3 + FA-7] compared against experimental measurements. Mean absolute error (*MAE*) of each prediction is shown in legends.
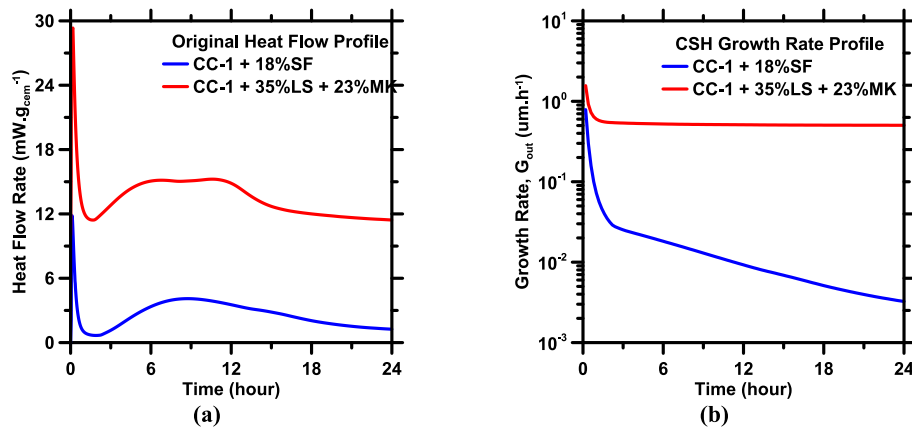

Fig. 5. (a) Original heat flow rate profiles and **(b)** C-S-H growth rate profiles of representative [PC + SCM]. The growth rate profiles have much simpler profile structure (i.e., low dimensionality); thereby making is easier for the advanced pBNG model to learn the input–output correlations.

kinetics, as the pBNG component can reproduce identical heat flow rate profiles from growth rate profiles. Additionally, the growth rate of C-S-H decreases nonlinearly by roughly two orders of magnitude during the first 24 h of hydration, which contributes to changes in the degree of saturation of C-S-H. The correlation between C-S-H's supersaturation and growth rate has been reported in previous studies [16,43,44,60]. At early stages, a high degree of saturation of C-S-H leads to a high driving force for nucleation and growth, resulting in faster growth rates. As the process continues and the degree of saturation of C-S-H decreases, the growth rate decelerates.

Having demonstrated the excellent prediction performance of the advanced pBNG model in predicting heat flow profiles of [PC + SCM],

we now seek to interpret the influences of various SCMs on the hydration of PC. Fig. 6 illustrates the calorimetric parameters and C-S-H growth rate, as derived from the advanced pBNG model, of PC replaced by individual SCMs. The calorimetric parameters are extracted from heat rate profiles through a customized MATLAB algorithm. It is worth noting that our database lacks calorimetry profiles of [PC + SF] beyond a replacement level of 30%. The FAs are classified into four categories: low reactivity (LR); low sulfur content (LS); high reactivity (HR); and high sulfur content (HS). Each of these categories exhibits a distinct pattern in its effect on the hydration kinetics of PC.

In Fig. 6a-c, it can be observed that QZ, SF, and LS can accelerate the hydration of PC. This is seen through shorter hydration times and more
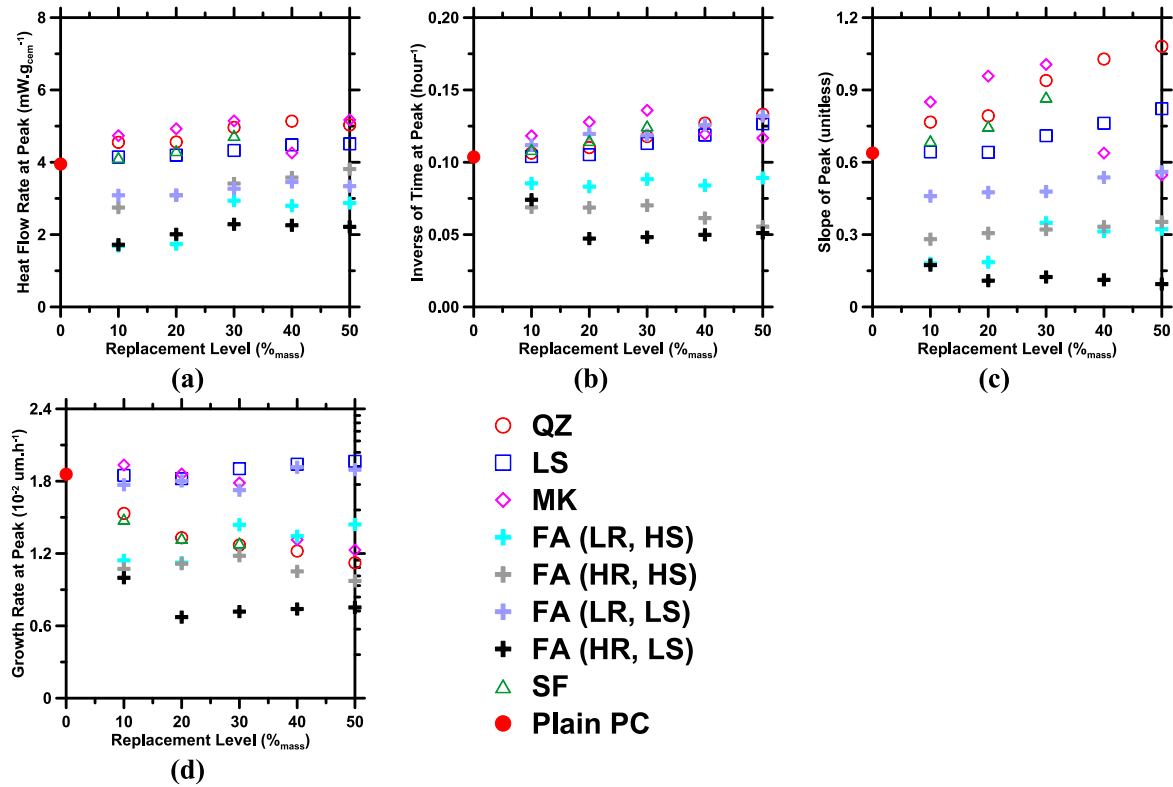
Fig. 6. **(a)** Maximum heat flow rate at the hydration peak; **(b)** inverse of the time of the maximum heat flow rate; **(c)** slope of hydration peak; and **(d)** C-S-H growth rate at hydration peak of PC replaced by individual SCMs at different replacement levels. LR = low reactivity; HR = high reactivity; LS = low sulfur; and HS = high sulfur.

intense hydration peaks as the replacement level of these SCMs is increased. This is expected as these SCMs provide additional surfaces for the nucleation and growth of C-S-H. However, the influence of the MK is different. Lapeyre and Kumar [16] have reported that there is a threshold of 30% replacement level for MK (also observed in this study), below which it acts as an inert SCM and exerts the filler effect to enhance PC's hydration. Beyond this threshold, MK releases sufficient $Al(OH)_4^-$ which partially covers the particles of PC and prevents them from coming into contact with water. Additionally, the aluminate ions combine with aqueous calcium (and hydroxyl and other) ions to form compounds such as ettringite or hydrogarnet. These effects—when combined—are expected to decelerate the precipitation of C-S-H; consequently, PC hydration slows down as the replacement level of MK is increased. Through a comparison of the slopes of the hydration peaks of binders, it is evident that the hydration of PC replaced by QZ, SF, and MK (before 30% replacement level) is more accelerated than when replaced by LS. This can be attributed to two reasons. First is the pozzolanic reaction, where the silicate ions released from silicate-based SCMs react with calcium ions to form pozzolanic C-S-H, leading to an acceleration of the hydration. Additionally, the SSAs of QZ (17677 $cm^2 \cdot g^{-1}$), SF (198000 $cm^2 \cdot g^{-1}$), and MK (5942 $cm^2 \cdot g^{-1}$) are higher than that of LS (1697 $cm^2 \cdot g^{-1}$), providing a greater surface for the heterogeneous nucleation of C-S-H. The influences of FAs on the hydration kinetics of PC are intricate due to broad-range variations in their chemical compositions (e.g., sulfur content) and molecular structure (e.g., network connectivity). FA (LR, LS) exhibits similar impacts on the hydration kinetics as QZ and LS, with hydration peaks occurring earlier as the replacement level increases. These FAs primarily provide the filler effect to accelerate the hydration of PC. However, the release of selected ions, such as $Al(OH)_4^-$ and sulfate, decelerates hydration, thereby decreasing the heat flow rate and slope of hydration peaks. As the replacement level of FA (LR, HS) increases, the hydration peak time does not show a significant change, but the intensity of the hydration peak increases when

the replacement level exceeds 20%. Despite its low reactivity, the high sulfur content of FA (LR, HS) leads to a continuous release of sulfate, which compensates for the filler effect through the formation of ettringite. However, in the range of 30–50% replacement level, the pozzolanic reaction partially overcomes the negative effects of sulfate release and slightly enhances the hydration of PC. When hydration begins, FA (HR, HS) releases a substantial amount of sulfate. Even at a 10% replacement level, the amount of sulfate released is enough to react with C_3A, meaning that increasing the replacement level further will not retard the hydration. However, as the replacement level increases, FA (HR, HS) releases more silicate and enhances the pozzolanic reaction, as evidenced by the high heat flow rate at the peak of hydration at higher replacement levels. Because of its low sulfur content, FA (HR, LS) is unable to release a significant amount of sulfate at the onset of hydration. Instead, it releases sulfate gradually throughout the hydration process, which results in a progressive formation of ettringite and significantly retard the hydration. It is important to note that all types of FAs release $Al(OH)_4^-$ which lessens the intensity of hydration. This can be observed by the downward shift in the heat flow rate and slope of peaks when compared to other SCMs.

In Fig. 6d, it is clear that the C-S-H growth rate of PC replaced by QZ and SF decreases as the replacement level increases. While these SCMs provide additional surfaces for C-S-H nucleation, excessive nuclei hasten the depletion of calcium ions. The C-S-H growth rate is closely tied to the availability of calcium ions. When the concentration of calcium ions is insufficient, the growth of C-S-H growth is hindered. This is further reinforced by the results of [PC + LS]; here, LS provides ample calcium ions through slow dissolution [75,76], resulting in little-to-no change in the growth rate. The release of calcium ions from MK helps to maintain the C-S-H growth rate. However, as the replacement level of MK increases, the high concentration of $Al(OH)_4^-$ from MK can inhibit the growth of C-S-H. Although the continual release of calcium ions, Al (OH)$_4^-$, and sulfate from FA (LR, LS), released levels of $Al(OH)_4^-$, and

sulfate are not high enough to impede the growth of C-S-H. As a result, the influence of FA (LR, LS) on the growth of C-S-H is similar to that of LS. For FA (LR, HS) and FA (HR, HS), sulfate is the dominant factor inhibiting the growth of C-S-H. Due to high reactivity, FA (HR, LS) releases a large amount of $Al(OH)_4^-$ to slow down the growth of C-S-H.

5. Conclusions

The reduction of carbon-footprint has become a major concern for researchers in the cement industry. One way to address this issue is by developing sustainable cementitious binders, which mitigates the CO_2 emissions associated with PC. One promising approach is the use of SCMs to replace a portion of the PC in the mixture design. SCMs can have a significant impact on the fresh and hardened properties of cement, determined by their chemical compositions and molecular structures. However, the complexity of SCMs has made it challenging for researchers to develop a reliable model for predicting the hydration kinetics of [PC + SCM] binders. The pBNG model is one such model that can reproduce the heat evolution profiles of [PC + SCM], but its extensive calibration and trial-and-error based estimation of parameters cannot be obtained directly from simple experiments. This highlights the ongoing need for further research to fully understand the science behind sustainable cementitious materials and to develop more reliable models to predict hydration kinetics.

This study introduces an advanced pBNG model, designed to accurately predict the heat flow rate profiles of [PC + SCM]. This model involves with a DF component to guess the critical parameter (i.e., growth rate of C-S-H) based on the mixture deign of sustainable cementitious binders. Consequently, the predicted parameter is implemented to the pBNG component to reproduce the heat evaluation profiles. The advanced pBNG model can produce reliable predictions, even when working with a small but highly diverse database. The database includes 710 cementitious binders made with 10 PCs (i.e., commercial and synthetic) and 14 common SCMs (i.e., QZ, LS, SF, MK, and FA). Results from this study show that the advanced pBNG model produces superior predictions compared to the DF model. Additionally, by simulating heat evolution profiles using a kinetic model, the final predictions avoid violating fundamental principles of material behavior. The study also investigates the ways in which different SCMs affect the hydration peak and growth rate of C-S-H. Among the SCMs studied, FAs were found to exhibit the most complex mechanisms for impacting hydration kinetics. Overall, this study represents a significant step forward in the development of advanced theory-based models. Artificial intelligence has significantly boosted the predictive capabilities of theory-based models, enabling them to be applied to a wider range of complex sustainable cementitious binders. Similar approaches also can be applied to predict other compliance and constructability metrics of sustainable cementitious systems.

CRediT authorship contribution statement

Taihao Han: Writing – review & editing, Writing – original draft, Methodology, Formal analysis, Conceptualization. **Jie Huang:** Writing – review & editing, Supervision, Funding acquisition. **Gaurav Sant:** Writing – review & editing, Supervision, Funding acquisition. **Narayanan Neithalath:** Writing – review & editing, Supervision, Funding acquisition. **Ashutosh Goel:** Writing – review & editing, Supervision, Funding acquisition. **Aditya Kumar:** Writing – review & editing, Supervision, Funding acquisition, Conceptualization.

Declaration of Competing Interest

The authors declare that they have no known competing financial interests or personal relationships that could have appeared to influence the work reported in this paper.

Data availability

Data will be made available on request.

Appendix A. Supplementary data

Supplementary data to this article can be found online at https://doi.org/10.1016/j.conbuildmat.2023.133327.

References

[1] A. Dowling, J. O'Dwyer, C.C. Adley, Lime in the limelight, J. Clean. Prod. 92 (2015) 13–22, https://doi.org/10.1016/j.jclepro.2014.12.047.

[2] F. Schorcht, Best available techniques (BAT) reference document for the production of cement, lime and magnesium oxide: industrial emissions directive. (2013). https://ec.europa.eu/jrc/en/publication/reference-reports/best-available-techniques-bat-reference-document-production-cement-lime-and-magnesium-oxide.

[3] M.M. Miller, Lime, United States Geological Survey, 2012 Minerals Yearbook, (2013).

[4] International Energy Agency, Renewable Energy for Industry, International Energy Agency, Paris, 2017 https://www.iea.org/reports/renewable-energy-for-industry.

[5] CEMEX, CEMEX and Synhelion achieve breakthrough in cement production with solar energy, (2022). https://www.cemex.com/-/cemex-and-synhelion-achieve-breakthrough-in-cement-production-with-solar-energy.

[6] The Business Research Company, Carbon Capture, Utilization, And Storage Global Market Report 2023, The Business Research Company, (2023).

[7] J. Davidovits, Geopolymers, J. Therm. Anal. 37 (1991) 1633–1656, https://doi.org/10.1007/BF01912193.

[8] J. Péra, J. Ambroise, New applications of calcium sulfoaluminate cement, Cem. Concr. Res. 34 (2004) 671–676, https://doi.org/10.1016/j.cemconres.2003.10.019.

[9] A.K. Misra, R. Mathur, Magnesium oxychloride cement concrete, Bull. Mater. Sci. 30 (2007) 239–246, https://doi.org/10.1007/s12034-007-0043-4.

[10] J.J. Biernacki, J.W. Bullard, G. Sant, K. Brown, F. Glasser, S. Jones, T. Ley, R. Livingston, L. Nicoleau, J. Olek, F. Sanchez, R. Shahsavari, P.E. Stutzman, K. Sobolev, T. Prater, et al., Cements in the 21st century: Challenges, perspectives, and opportunities, J. Am. Ceram. Soc. 100 (7) (2017) 2746–2773.

[11] M. Juenger, J.L. Provis, J. Elsen, W. Matthes, R.D. Hooton, J. Duchesne, L. Courard, H. He, F. Michel, R. Snellings, et al., Supplementary cementitious materials for concrete: characterization needs, MRS Online Proc. Libr. 1488 (2012) 8–22, https://doi.org/10.1016/j.cemconres.2019.05.008.

[12] M.C.G. Juenger, R. Snellings, S.A. Bernal, Supplementary cementitious materials: new sources, characterization, and performance insights, Cem. Concr. Res. 122 (2019) 257–273, https://doi.org/10.1016/j.cemconres.2019.05.008.

[13] M.C.G. Juenger, R. Siddique, Recent advances in understanding the role of supplementary cementitious materials in concrete, Cem. Concr. Res. 78 (Part A) (2015) 71–80, https://doi.org/10.1016/j.cemconres.2015.03.018.

[14] M.A. Megat Johari, J.J. Brooks, S. Kabir, P. Rivard, Influence of supplementary cementitious materials on engineering properties of high strength concrete, Constr. Build. Mater. 25 (5) (2011) 2639–2648.

[15] H. Toutanji, N. Delatte, S. Aggoun, R. Duval, A. Danson, Effect of supplementary cementitious materials on the compressive strength and durability of short-term cured concrete, Cem. Concr. Res. 34 (2004) 311–319, https://doi.org/10.1016/j.cemconres.2003.08.017.

[16] J. Lapeyre, A. Kumar, Influence of pozzolanic additives on hydration mechanisms of tricalcium silicate, J. Am. Ceram. Soc. 101 (2018) 3557–3574, https://doi.org/10.1111/jace.15518.

[17] R. Cook, H. Ma, A. Kumar, Influence of size-classified and slightly soluble mineral additives on hydration of tricalcium silicate, J. Am. Ceram. Soc. 103 (2020) 2764–2779, https://doi.org/10.1111/jace.16936.

[18] X. Guo, J. Yang, G. Xiong, Influence of supplementary cementitious materials on rheological properties of 3D printed fly ash based geopolymer, Cem. Concr. Compos. 114 (2020), 103820, https://doi.org/10.1016/j.cemconcomp.2020.103820.

[19] T. Oey, A. Kumar, J.W. Bullard, N. Neithalath, G. Sant, G. Scherer, The filler effect: the influence of filler content and surface area on cementitious reaction rates, J. Am. Ceram. Soc. 96 (6) (2013) 1978–1990.

[20] A. Kumar, T. Oey, S. Kim, D. Thomas, S. Badran, J. Li, F. Fernandes, N. Neithalath, G. Sant, Simple methods to estimate the influence of limestone fillers on reaction and property evolution in cementitious materials, Cem. Concr. Compos. 42 (2013) 20–29, https://doi.org/10.1016/j.cemconcomp.2013.05.002.

[21] D.P. Bentz, O.M. Jensen, A.M. Coats, F.P. Glasser, Influence of silica fume on diffusivity in cement-based materials: I Experimental and computer modeling

studies on cement pastes, Cement and Concrete Research 30 (2000) 953–962, https://doi.org/10.1016/S0008-8846(00)00264-7.

[22] J. Lapeyre, H. Ma, A. Kumar, Effect of particle size distribution of metakaolin on hydration kinetics of tricalcium silicate, J. Am. Ceram. Soc. 102 (2019) 5976–5988, https://doi.org/10.1111/jace.16467.

[23] J.W. Bullard, H.M. Jennings, R.A. Livingston, A. Nonat, G.W. Scherer, J. S. Schweitzer, K.L. Scrivener, J.J. Thomas, Mechanisms of cement hydration, Cem. Concr. Res. 41 (2011) 1208–1223, https://doi.org/10.1016/j.cemconres.2010.09.011.

[24] J.J. Thomas, J.J. Biernacki, J.W. Bullard, S. Bishnoi, J.S. Dolado, G.W. Scherer, A. Luttge, Modeling and simulation of cement hydration kinetics and microstructure development, Cem. Concr. Res. 41 (2011) 1257–1278, https://doi.org/10.1016/j.cemconres.2010.10.004.

[25] R. Cook, H. Ma, M. Okoronkwo, G. Sant, A. Kumar, Influence of water activity on belite (β-C2S) hydration, J. Am. Ceram. Soc. 104 (2021) 1831–1840, https://doi.org/10.1111/jace.17608.

[26] E. Breval, C₃A hydration, Cem. Concr. Res. 6 (1976) 129–137, https://doi.org/10.1016/0008-8846(76)90057-0.

[27] A. Quennoz, K.L. Scrivener, Hydration of C₃A–gypsum systems, Cem. Concr. Res. 42 (2012) 1032–1041, https://doi.org/10.1016/j.cemconres.2012.04.005.

[28] A.I. Vovk, Hydration of tricalcium aluminate C₃A and C₃A-gypsum mixtures in the presence of surfacants: adsorption or surface phase formation? Colloid J. 62 (2000) 24–31.

[29] J. Lapeyre, H. Ma, M. Okoronkwo, G. Sant, A. Kumar, Influence of water activity on hydration of tricalcium aluminate-calcium sulfate systems, J. Am. Ceram. Soc. 103 (6) (2020) 3851–3870.

[30] A. Kumar, S. Bishnoi, K.L. Scrivener, Modelling early age hydration kinetics of alite, Cem. Concr. Res. 42 (2012) 903–918, https://doi.org/10.1016/j.cemconres.2012.03.003.

[31] I.A. Chen, M.C. Juenger, Synthesis and hydration of calcium sulfoaluminate-belite cements with varied phase compositions, J. Mater. Sci. 46 (2011) 2568–2577, https://doi.org/10.1007/s10853-010-5109-9.

[32] R. Cook, T. Han, A. Childers, C. Ryckman, K. Khayat, H. Ma, J. Huang, A. Kumar, Machine learning for high-fidelity prediction of cement hydration kinetics in blended systems, Mater. Des. 208 (2021), 109920, https://doi.org/10.1016/j.matdes.2021.109920.

[33] J. Lapeyre, T. Han, B. Wiles, H. Ma, J. Huang, G. Sant, A. Kumar, Machine learning enables prompt prediction of hydration kinetics of multicomponent cementitious systems, Sci. Rep. 11 (2021) 3922, https://doi.org/10.1038/s41598-021-83582-6.

[34] T. Han, S.A. Ponduru, R. Cook, J. Huang, G. Sant, A. Kumar, A Deep learning approach to design and discover sustainable cementitious binders: Strategies to learn from small databases and develop closed-form analytical models, Front. Mater. 8 (2022), 796476, https://doi.org/10.3389/fmats.2021.796476.

[35] T. Han, R. Bhat, S.A. Ponduru, A. Sarkar, J. Huang, G. Sant, H. Ma, N. Neithalath, A. Kumar, Deep learning to predict the hydration and performance of fly ash-containing cementitious binders, Cem. Concr. Res. 165 (2023), 107093, https://doi.org/10.1016/j.cemconres.2023.107093.

[36] L. Nicoleau, A. Nonat, A new view on the kinetics of tricalcium silicate hydration, Cem. Concr. Res. 86 (2016) 1–11, https://doi.org/10.1016/j.cemconres.2016.04.009.

[37] P. Juilland, E. Gallucci, R. Flatt, K. Scrivener, Dissolution theory applied to the induction period in alite hydration, Cem. Concr. Res. 40 (2010) 831–844, https://doi.org/10.1016/j.cemconres.2010.01.012.

[38] A.M. Ley-Hernandez, J. Lapeyre, R. Cook, A. Kumar, D. Feys, Elucidating the effect of water-to-cement ratio on the hydration mechanisms of cement, ACS Omega 3 (2018) 5092–5105, https://doi.org/10.1021/acsomega.8b00097.

[39] G.W. Scherer, J. Zhang, J.J. Thomas, Nucleation and growth models for hydration of cement, Cem. Concr. Res. 42 (2012) 982–993, https://doi.org/10.1016/j.cemconres.2012.03.019.

[40] J.J. Thomas, H.M. Jennings, J.J. Chen, Influence of nucleation seeding on the hydration mechanisms of tricalcium silicate and cement, J. Phys. Chem. C 113 (2009) 4327–4334, https://doi.org/10.1021/jp809811w.

[41] J.J. Thomas, A new approach to modeling the nucleation and growth kinetics of tricalcium silicate hydration, J. Am. Ceram. Soc. 90 (2007) 3282–3288, https://doi.org/10.1111/j.1551-2916.2007.01858.x.

[42] G.W. Scherer, Models of confined growth, Cem. Concr. Res. 42 (2012) 1252–1260, https://doi.org/10.1016/j.cemconres.2012.05.018.

[43] W. Meng, P. Lunkad, A. Kumar, K. Khayat, Influence of silica fume and polycarboxylate ether dispersant on hydration mechanisms of cement, J. Phys. Chem. C 120 (2016) 26814–26823, https://doi.org/10.1021/acs.jpcc.6b08121.

[44] J.W. Bullard, G.W. Scherer, J.J. Thomas, Time dependent driving forces and the kinetics of tricalcium silicate hydration, Cem. Concr. Res. 74 (2015) 26–34, https://doi.org/10.1016/j.cemconres.2015.03.016.

[45] F. Bellmann, G.W. Scherer, Analysis of C-S-H growth rates in supersaturated conditions, Cem. Concr. Res. 103 (2018) 236–244, https://doi.org/10.1016/j.cemconres.2017.05.007.

[46] A. Bazzoni, H. Ma, Q. Wang, X. Shen, M. Cantoni, K.L. Scrivener, G. Scherer, The effect of magnesium and zinc ions on the hydration kinetics of C₃S, J. Am. Ceram. Soc. 97 (11) (2014) 3684–3693.

[47] K. O. Akande, T. O. Owolabi, S. Twaha, S.O. Olatunji, Performance comparison of SVM and ANN in predicting compressive strength of concrete, IOSR Journal of Computer Engineering. 16 (5) (2014) 88–94.

[48] A. Behnood, V. Behnood, M.M. Gharehveran, K.E. Alyamac, Prediction of the compressive strength of normal and high-performance concretes using M5P model tree algorithm, Constr. Build. Mater. 142 (2017) 199–207.

[49] J.-S. Chou, C.-K. Chiu, M. Farfoura, I. Al-Taharwa, Optimizing the prediction accuracy of concrete compressive strength based on a comparison of data-mining techniques, J. Comput. Civ. Eng. 25 (3) (2011) 242–253.

[50] J.-S. Chou, C.-F. Tsai, A.-D. Pham, Y.-H. Lu, Machine learning in concrete strength simulations: multi-nation data analytics, Constr. Build. Mater. 73 (2014) 771–780, https://doi.org/10.1016/j.conbuildmat.2014.09.054.

[51] Z.-H. Duan, S.-C. Kou, C.-S. Poon, Prediction of compressive strength of recycled aggregate concrete using artificial neural networks, Constr. Build. Mater. 40 (2013) 1200–1206, https://doi.org/10.1016/j.conbuildmat.2012.04.063.

[52] R. Gupta, M.A. Kewalramani, A. Goel, Prediction of concrete strength using neural-expert system, J. Mater. Civ. Eng. 18 (2006) 462–466, https://doi.org/10.1061/(ASCE)0899-1561(2006)18:3(462).

[53] S. Nazar, J. Yang, A. Ahmad, S.F.A. Shah, Comparative study of evolutionary artificial intelligence approaches to predict the rheological properties of fresh concrete, Mater. Today Commun. 32 (2022), 103964, https://doi.org/10.1016/j.mtcomm.2022.103964.

[54] D. Sathyan, D. Govind, C.B. Rajesh, K. Gopikrishnan, G. Aswath Kannan, J. Mahadevan, Modelling the Shear flow behaviour of cement paste using machine learning –XGBoost, J. Phys. Conf. Ser. 1451 (1) (2020), 012026, https://doi.org/10.1088/1742-6596/1451/1/012026.

[55] L. Nicoleau, A. Nonat, D. Perrey, The di- and tricalcium silicate dissolutions, Cem. Concr. Res. 47 (2013) 14–30, https://doi.org/10.1016/j.cemconres.2013.01.017.

[56] H. Minard, S. Garrault, L. Regnaud, A. Nonat, Mechanisms and parameters controlling the tricalcium aluminate reactivity in the presence of gypsum, Cem. Concr. Res. 37 (2007) 1418–1426, https://doi.org/10.1016/j.cemconres.2007.06.001.

[57] A. Quennoz, K.L. Scrivener, Interactions between alite and C3A-gypsum hydrations in model cements, Cem. Concr. Res. 44 (2013) 46–54, https://doi.org/10.1016/j.cemconres.2012.10.018.

[58] J.W. Bullard, A determination of hydration mechanisms for tricalcium silicate using a kinetic cellular automaton model, J. Am. Ceram. Soc. 91 (2008) 2088–2097, https://doi.org/10.1111/j.1551-2916.2008.02419.x.

[59] J.W. Bullard, R.J. Flatt, New insights into the effect of calcium hydroxide precipitation on the kinetics of tricalcium silicate hydration, J. Am. Ceram. Soc. 93 (2010) 1894–1903, https://doi.org/10.1111/j.1551-2916.2010.03656.x.

[60] T. Oey, A. Kumar, G. Falzone, J. Huang, S. Kennison, M. Bauchy, N. Neithalath, J. W. Bullard, G. Sant, L. Struble, The influence of water activity on the hydration rate of tricalcium silicate, J. Am. Ceram. Soc. 99 (7) (2016) 2481–2492.

[61] H.G. Dawson, On the Numerical Value of ∫0hex2dx, Proc. Lond. Math. Soc. s1-29 (1) (1897) 519–522.

[62] D.R.G. Mitchell, I. Hinczak, R.A. Day, Interaction of silica fume with calcium hydroxide solutions and hydrated cement pastes, Cem. Concr. Res. 28 (1998) 1571–1584, https://doi.org/10.1016/S0008-8846(98)00133-1.

[63] E.D. Rodríguez, L. Soriano, J. Payá, M.V. Borrachero, J.M. Monzó, Increase of the reactivity of densified silica fume by sonication treatment, Ultrason. Sonochem. 19 (2012) 1099–1107, https://doi.org/10.1016/j.ultsonch.2012.01.011.

[64] A.J. Allen, J.J. Thomas, H.M. Jennings, Composition and density of nanoscale calcium–silicate–hydrate in cement, Nat. Mater. 6 (2007) 311–316, https://doi.org/10.1038/nmat1871.

[65] J.J. Thomas, H.M. Jennings, A.J. Allen, Relationships between composition and density of tobermorite, jennite, and nanoscale CaO−SiO₂−H₂O, J. Phys. Chem. C 114 (2010) 7594–7601, https://doi.org/10.1021/jp910733x.

[66] J.A. Nelder, R. Mead, A simplex method for function minimization, Comput. J. 7 (4) (1965) 308–313.

[67] K.I.M. McKinnon, Convergence of the Nelder-Mead Simplex Method to a Nonstationary Point, SIAM J. Optim. 9 (1998) 148–158, https://doi.org/10.1137/S1052623496303482.

[68] T. Han, E. Gomaa, A. Gheni, J. Huang, M. ElGawady, A. Kumar, Machine learning enabled closed-form models to predict strength of alkali-activated systems, J. Am. Ceram. Soc. 105 (2022) 4414–4425, https://doi.org/10.1111/jace.18399.

[69] R. Bhat, T. Han, S. Akshay Ponduru, A. Reka, J. Huang, G. Sant, A. Kumar, Predicting compressive strength of alkali-activated systems based on the network topology and phase assemblages using tree-structure computing algorithms, Constr. Build. Mater. 336 (2022), 127557, https://doi.org/10.1016/j.conbuildmat.2022.127557.

[70] K. De Weerdt, M.B. Haha, G. Le Saout, K.O. Kjellsen, H. Justnes, B. Lothenbach, Hydration mechanisms of ternary Portland cements containing limestone powder and fly ash, Cem. Concr. Res. 41 (2011) 279–291, https://doi.org/10.1016/j.cemconres.2010.11.014.

[71] P.K. Mehta, P.J. Monteiro, Concrete-Microstructure, Properties and Materials. (2006).

[72] H.F.W. Taylor, Cement Chemistry, Thomas Telford, 1997.

[73] I. Mehdipour, A. Kumar, K.H. Khayat, Rheology, hydration, and strength evolution of interground limestone cement containing PCE dispersant and high volume supplementary cementitious materials, Mater. Des. 127 (2017) 54–66, https://doi.org/10.1016/j.matdes.2017.04.061.

[74] E. Masoero, J.J. Thomas, H.M. Jennings, G. Scherer, A reaction zone hypothesis for the effects of particle size and water-to-cement ratio on the early hydration kinetics of C₃S, J. Am. Ceram. Soc. 97 (3) (2014) 967–975.

[75] B. Lothenbach, G. Le Saout, E. Gallucci, K. Scrivener, Influence of limestone on the hydration of Portland cements, Cem. Concr. Res. 38 (2008) 848–860, https://doi.org/10.1016/j.cemconres.2008.01.002.

[76] J. Péra, S. Husson, B. Guilhot, Influence of finely ground limestone on cement hydration, Cem. Concr. Compos. 21 (1999) 99–105, https://doi.org/10.1016/S0958-9465(98)00020-1.